JOURNAL OF MAGNETIC RESONANCE IMAGING 25:279–289 (2007)

Invited Review

Magnetic Resonance Imaging With Ultrashort TE (UTE) PULSE Sequences: Technical Considerations

Damian J. Tyler, PhD,[1] Matthew D. Robson, PhD,[1] R. Mark Henkelman, PhD,[2] Ian R. Young, PhD,[3] and Graeme M. Bydder, MB, ChB[4]*

It is now possible to detect signals from tissues and tissue components with short T_2s, such as cortical bone, using ultrashort TE (UTE) pulse sequences. The background to the use of these sequences is reviewed with particular emphasis on MR system issues. Tissue properties are discussed, and tissues are divided into those with a majority and those with a minority of short T_2 components. UTE pulse sequences and their variants are described and clinical applications are illustrated. System design requirements for sequences of this type, including gradient performance, RF switching, and data-processing issues, are outlined.

Key Words: magnetic resonance imaging; ultrashort echo times; pulse sequences; short T_2, musculoskeletal tissue
J. Magn. Reson. Imaging 2007;25:279–289.

A VARIETY OF TISSUE COMPONENTS have short T_2s. Their MR signal decays rapidly, and thus little or no signal is detectable by the time conventional MR systems begin to operate in receive mode. They therefore appear dark with virtually all pulse sequences routinely used in clinical MRI. Pulse sequences with echo times (TEs) 10–200 times shorter than those normally used on conventional clinical systems are now being implemented and can detect signals from tissues with short T_2s (1–14). These sequences provide new options for characterizing tissue and manipulating conspicuity. In this paper we describe the basic physics underlying ultrashort TE (UTE) pulse sequences, and illustrate some clinical applications of this technique. Design requirements for the use of pulse sequences of this type on clinical MR systems are emphasized.

BASIC PHYSICS

Excited Signal

The observed signal S_o produced by MR excitation is given by

$$S_o = K\rho\sum c_r f(T_{1r},T_{2r}), \quad (1)$$

where ρ is the total proton density (PD) (assuming that protons are the target nucleus, although this is equally applicable to other nuclei), and c_r, T_{1r}, T_{2r} are respectively the fraction of the PD and the effective relaxation time constants of the rth component of the tissue being imaged. K is a scaling factor relating the PD to the measured signal, and $f(T_{1r},T_{2r})$ is a term describing the response of the rth component to the imaging sequence in use, assuming that the effects of exchange processes on MR signals can be represented as variations in time constants.

The simplest relationship that is appropriate for a single component in an MR image is:

$$S_o = KF\rho\exp(-TE/T_2)\sin\alpha(1-\exp(-TR/T_1))/(1-\cos\beta\exp(-TR/T_1)), \quad (2)$$

where TR is the sequence repetition time in a selective excitation procedure, and TE is taken to be the time between the central point of the excitation process that rotates the magnetization into the XY plane and the time at which the central point of the data k-space is sampled. Conventionally this is known as the "echo time" because practical data-recovery procedures usually involve the formation of an echo by one mechanism or another. When this relationship is generalized from the Ernst angle formulation (15), there are implicit assumptions that the excitation is on resonance, and that T_2 is long compared to the excitation process.

We define α as the "flip angle" that is actually achieved by the excitation, while β ($>\alpha$) is a shorthand representation of a complex relationship that includes the effects of off-resonance excitation on broad lines as well as transverse relaxation of signals during the ra-

[1]Oxford University Centre for Clinical Magnetic Resonance Research, MRS Unit, John Radcliffe Hospital, Oxford, United Kingdom.
[2]Mouse Imaging Center, Hospital for Sick Children, Toronto, Ontario, Canada.
[3]Department of Electrical Engineering, Imperial College London, United Kingdom.
[4]Department of Radiology, University of California–San Diego, San Diego, California, USA.
*Address reprint requests to: G.M.B., Department of Radiology, University of California–San Diego, 200 West Arbor Drive, San Diego, CA 92103-8226. E-mail: gbydder@ucsd.edu
Received July 3, 2006; Accepted September 28, 2006.
DOI 10.1002/jmri.20851
Published online in Wiley InterScience (www.interscience.wiley.com).

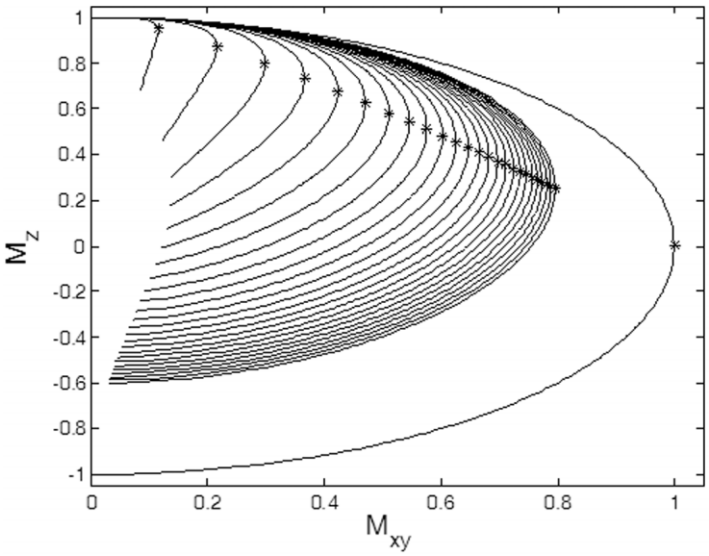

Figure 1. Simulation of the behavior of the spin system in response to a 180° hard pulse of 500 μs duration (the equivalent of a 1 kHz B_1 field). The curved trajectory starting at $M_z = 1$ and $M_{xy} = 0$ shows the evolving magnetization as the RF pulse duration increases from 0° to 180° for a series of components of different T_2s ranging from 20 to 500 μs in 20-μs intervals. A component with a long T_2 of 100 msec is shown for comparison. The * sign shows where the maximum transverse signal is obtained. These data are replotted in a more convenient form in Fig. 2.

diofrequency (RF) pulse. The signal in an image is the spatial integration over a voxel containing protons that are affected differently by the pulse sequence, and the term "F" is designed to accommodate this. It includes, for example, effects on slice shape for a particular flip angle, and the relative sizes of T_1 and TR. The recovered signal is also affected by the way in which neighboring regions of tissue are manipulated and imaged. Many of these interactions are themselves dependent on the relaxation time constants, and hence may be expected to affect individual components with different T_1s and T_2s to different extents.

Excitation of the Magnetization of Short T_2 Relaxation Components

As suggested above, and described previously (16), excitation is more complex when RF pulses durations are similar to or longer than the T_2 of the components being excited. Relaxation during the RF pulse results in a reduction of the magnetization available in the transverse plane without a compensatory increase in the available magnetization in the longitudinal plane. In effect, there is competition between the RF pulse that rotates the magnetization into the XY plane, and the dephasing that occurs within that plane. The impact of the loss of magnetization is illustrated in Fig. 1, which shows a simulation based on the use of a 500-μs-duration hard 180° pulse, which is typical of those available on clinical systems. The B_1 field in this instance is about 23.5 μT. Figure 2 shows a rearrangement of the data from Fig. 1 and illustrates that the maximum effective signal for short T_2 components is obtained with RF excitations that would conventionally be expected to produce substantially less than a 90° rotation. Note, however, that an increase in pulse amplitude effectively compresses the curve in Fig. 2 toward the left.

Another consequence of relaxation during excitation is that for long RF pulses, the transverse magnetization "forgets" about earlier stages of the RF pulse. Thus, transverse magnetization is weighted toward the end of a long RF pulse, and measuring TE from the center of the pulse is inaccurate. This effect is present when T_2 is long (with the true value of TE slightly shorter than might be assumed using the pulse center as a reference), but is much more significant when T_2 is short. The "forgetful" nature of the transverse magnetization also means that it is insensitive to the early (and hence high) spatial frequency parts of the excitation pulse. This effect tends to blur sharp slice-selection boundaries when short T2 components are imaged.

Inversion

As noted above, the change in longitudinal magnetization after excitation into the transverse plane is less than might be expected, and, as Fig. 1 suggests, it may be very difficult to invert short T_2 components at all. The key to achieving inversion is that the excited magneti-

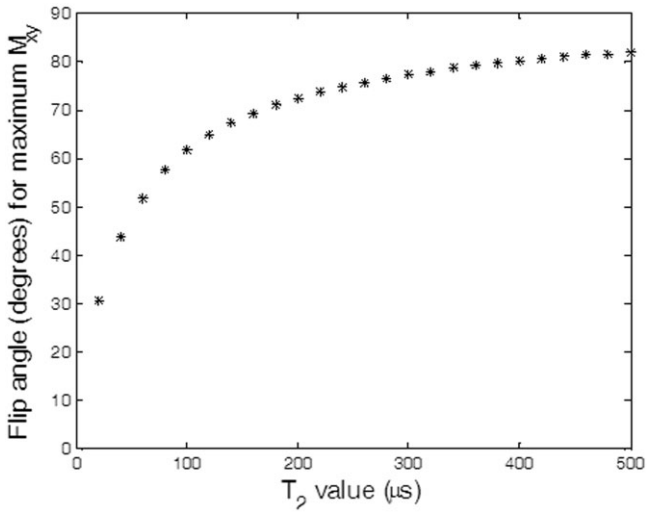

Figure 2. Plot of the optimum RF pulse duration (conventional flip angle α) to obtain the highest signal at different values of T_2 using the same simulated values as in Fig. 1. The effective rotation of the magnetization is much less than α for short T_2 components.

Table 1
Saturation Strategies in UTE Imaging

Method	How does it work	Limitations
Long hard pulse on resonance with spoiler	Saturates all pools	RF power limitations
Short 90° pulse on resonance with spoiler	Excites all pools and dephases signals	No total short T_2 component saturation
Long 90° pulse on resonance with spoiler	Saturates the long T_2 pool; Leaves short T_2 pool	Not total short T_2 component saturation
Short 270° pulse on resonance with spoiler	Saturates long T_2 pools; Saturates short T_2 pools better than 90° approach	Partial inversion of intermediate T_2 species
Long hard pulse off-resonance	Leaves long T_2; Saturates short T_2	RF power limitations, implications for multislice imaging

zation should remain for the minimum possible time in the transverse plane. This emphasizes the need for powerful B_1 fields.

With an inversion pulse, long T_2 components are fully inverted. For short T_2 components, some spins (such as those within the bandwidth of the RF pulse or exchanging with such spins) behave as though they had been saturated by the inverting RF pulse, while others behave as though there had been no inverting pulse at all.

Expressing the process in a series of relationships illustrates the extent of the differences that may arise. Thus, the long T_2 components in effect obey the following relationship:

$$S_{on} = K\rho_n \exp[(-TE/T_{2n})(1 - 2\exp(-TI/T_{1n})) + \exp(-TR/T_{1n})], \quad (3)$$

where S_{on} is the observed signal for a narrow line component, K is a scaling factor relating PD and signal, ρ_n is the narrow component PD, and the "n" (narrow line) suffix relates to the properties of the long T_2 component.

Some spins within the bandwidth of the RF pulse or exchanging with such spins behave as though they had been saturated by the inverting RF pulse, so that:

$$S_{ow} = K_A\rho_w \exp[(-TE/T_{2w})(1 - \exp(-TI/T_{1w})], \quad (4a)$$

where the parameters in the relationship are as described above, with the difference that the "w" suffix refers to short T_2 components with wide spectral linewidths.

The rest of the short T_2 components behave as though there had been no inversion pulse at all, and, possibly, only a very limited degree of saturation, so that:

$$S_{ow} = K_B\rho_w \exp(-TE/T_{2w})(1-\exp(-TR/T_{1w}). \quad (4b)$$

One can invert the whole spin population by making the inversion pulse very short in relation to T_2. However, this is not applicable to interleaved multislice studies, since the bandwidth has to be very broad to ensure full inversion. If the short T_2 components are of greatest interest, long inversion pulses may be included to invert and null long T_2 components, although there may be some saturation of the residual short T_2 components.

Saturation

While inversion may be difficult to accomplish, saturation is readily achievable with the use of long, high-power RF pulses. With very short T_2 components alone, no crusher gradients at all may be needed. The effects of different strategies for saturation are summarized in Table 1.

Off-Resonance Effects

The line shapes of the components present may vary widely in width (i.e., components that are normally observed by MRI are narrow, and those that are usually invisible to MRI are broad).

In a conventional multislice spin-echo (SE) acquisition (17) the slices are excited in an interleaved manner. The selection process uses a constant field gradient, and the frequency of the RF excitation pulses is changed for different slices. Since the spread of a broad-line component may be tens of kHz, this type of excitation may affect spins in adjacent slices. This effect has been described for conventional sequences (18,19), but it affects short T_2 (broad-line) components to a much greater degree. To prevent this effect from reducing the signal, the slices must be distributed relatively widely (e.g., separated by 6 kHz, as in the implementation discussed here). This results in no detectable loss of signal from cortical bone ($T_2 \sim 420$ μs) in a multislice experiment. However, with this frequency offset there is a reduction (5–10%) in the signal from skeletal muscle due to magnetization transfer (MT) effects involving the short T_2 components of the muscle ($T_2 \sim 50$ μs), which is consistent with previous findings (20). All forms of spin manipulation using RF pulses can result in this type of problem. For example, even simple sequences such as SE and inversion recovery (IR) can induce changes in the broad lines, as can fat-suppression methods that rely on RF pulses. An 18% reduction in cortical bone signal intensity may be seen after the application of a fat-saturation pulse 230 Hz off-resonance. A relatively large effect is seen due to the close proximity of the saturation pulse to the resonance frequency. True off-resonance excitation does not result in any net magnetization being created in the transverse plane, and thus there is no signal available from this source.

Figure 3 illustrates the effect of applying long excitation pulses to two components: one with a T_2 of 400 μs

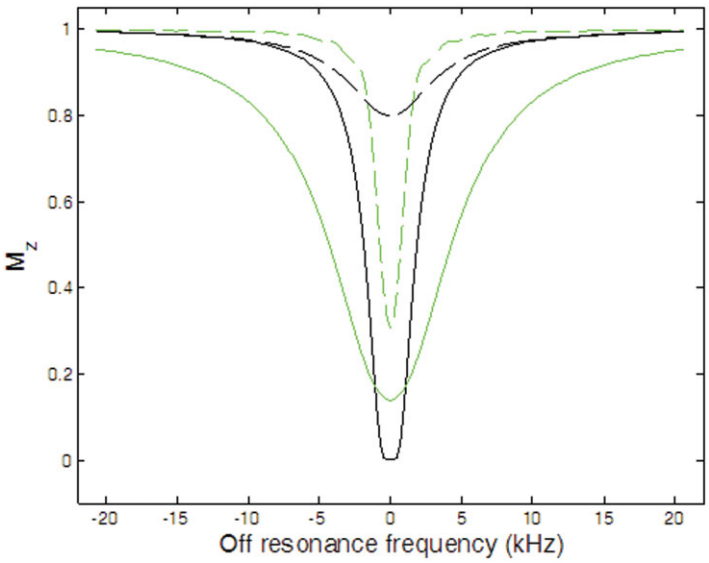

Figure 3. Simulation showing the residual longitudinal magnetization after excitation with a rectangular 0.5-msec 90° pulse (dashed) and a 4-msec 720° pulse (solid). The plot shows the effect of moving the excitation pulse off-resonance. Two T_2 values (50 μs (gray) and 40 μs (black)) are shown.

(typical of cortical bone), and the other with a shorter T_2 component of 50 μs (typical of skeletal muscle). The 90° pulse could be considered to be representative of a simple chemical shift-selective (CHESS) pulse (21) if it were applied in a 1.5T system at 230 Hz off-resonance.

The saturating effect due to RF irradiation on any Lorentzian-shaped line is given by (22):

$$S_{RF}/S_o = 1/(1 + \tan^2\Theta T_1/T_2), \quad (5)$$

in circumstances where $\gamma^2B_1{}^2T_1T_2 >> 1$ $\tan\Theta = B_1/\delta B_0$, where δB_0 is the offset field from resonance at which the RF irradiation of magnitude B_1 is applied, and S_{RF} is the signal observed in the presence of the RF irradiation.

Either individually or cumulatively, off-resonance excitation may produce changes that are otherwise indistinguishable from those of a deliberate MT sequence in which prolonged off-resonance RF irradiation is used to saturate broad-line spins. As previously shown by Forsen and Hoffman (23), this has the effect of reducing the apparent magnetization of the visible pool through the relationship:

$$S_o = (S_R - S_S)\exp(-t/T_{1S}) + S_S \quad (6)$$

where S_R is the signal observed immediately after excitation following a very long magnetization recovery time, S_S is the signal obtained after a very long period of irradiation, t is the duration of the RF irradiation, and T_{1S} is the time constant with which saturation is approached.

There are similarities in the use of UTE sequences and MT techniques due to the fact that they both probe the behavior of short T_2 species. In the case of MT experiments, a two-pool system is generally assumed (one pool is associated with free protons, and the other with restricted protons or protons contained within large molecules). The free proton pool has a long T_2 of 50–100 msec, and the restricted pool has a short T_2 of 10–250 μs. With conventional MT imaging sequences, the restricted proton pool is "invisible" and can only be investigated via exchange processes with the "visible" free pool. This leads to images that are weighted by the relative sizes of the two pools and the rate of magnetization exchange between them. Conversely, UTE sequences image the bound proton pool directly, and therefore yield images that are weighted by the actual size of the bound proton pool and its transverse relaxation rate.

UTE and MT methods are both applicable to spin systems in which the signal is not imaged by conventional techniques (e.g., $T_2 < 500$ μs). Of these two methods, the UTE method is strongest at the longer end of the range (e.g., ≥100 μs), whereas the MT approach can be applied to tissues with much shorter T_2s. However, the combination of MT techniques and UTE imaging sequences could yield more information than the two techniques applied separately. In this situation, two distinct cases can be envisioned:

1. The short T_2 pool is relatively isolated from any other pool, and little or no exchange takes place (e.g., in cortical bone).
2. There is a free and rapid exchange between the short T_2 pool and other pools (e.g., in skeletal muscle).

In the first case the combination of MT and UTE may not be practically useful, because the application of MT pulses would saturate the bound proton pool and leave no signal with which to create images (although MT could be used to create T_2 contrast within the short T_2 pool). For example, the application of a single MT pulse applied 1500 Hz off-resonance, equivalent to a 540° pulse applied on-resonance, leads to a 26% reduction in the available signal from cortical bone.

In the second case the combination of MT and UTE may provide more information about the rates of magnetization exchange between the short T_2 pool and any other pools present. In a system with a long T_2 component and a short T_2 component, as previously investigated using MT alone, a combined UTE and MT se-

quence could allow investigation of the recovery of the bound pool after saturation via exchange with the free pool. In a system with a short T_2 pool ($T_2 \sim 500$ μs) and a very short T_2 pool, <10 μs, a combined UTE and MT sequence could provide information about the very short T_2 pool that is "invisible" with current techniques.

$T_{1\rho}$ Effects

$T_{1\rho}$ is a parameter that is studied with the use of prolonged RF irradiation. One usually performs such studies by locking the excited spins to precess around the appropriately phased RF for periods typically on the order of T_2. Thereafter, the data are usually recovered using conventional gradient-recalled echo (GRE) sequences (24). $T_{1\rho}$ is a measure of what the T_1 of the component being studied would have been at very low field. It is generally substantially shorter than the observed T_1, and equals T_2 at the very lowest fields. If the frequency of the spin-locking pulse is off-resonance, the signals will appear to have another time constant $T_{1\rho off}$, where $T_2 < T_{1\rho} < T_{1\rho off} < T_1$. Shaped RF pulses that are being used to excite other slices could very well partially excite and then lock a broad line in another region. This is not very likely with simple pulses, where the phases of the irradiation are constrained to be either 0° or 180°, but as the pulse structure becomes complex with the phase of the RF being varied quasi-continuously, it becomes possible.

Magic Angle Effects

While it is technically difficult to acquire the signals from short T_2 components, there are circumstances in which alternative strategies can be of assistance. These arise principally when the mechanism that determines T_2 is ordered dipolar coupling (25). It has been observed that this form of coupling exists between collagen and water (26,27), and as a result this is the predominant effect that determines the appearance of tendons and ligaments on images (28). The relationship that determines the extent of dipolar coupling arises from classic magnetism theory regarding the energetics of the interaction between two dipoles, and takes the form:

$$B_I = \pm (\mu_0/4\pi)\mu(3\cos^2\Theta - 1)/r^3. \quad (7)$$

B_I is the change in observed field at the nucleus due to a dipole of strength μ at a distance r, where Θ is the angle between r and B_0 (the first term is a conversion to SI units). Ultimately, this relationship can be used to demonstrate that the magnitude of the effective value of T_2 depends on the angle between the two dipoles, and the main magnetic field. T_2 is at a maximum when the angle Θ is given by:

$$3\cos^2\Theta - 1 = 0 \quad (8)$$

(or when $\Theta = 54.7°$). Changing the orientation of certain tissues to the magnetic field can result in dramatic changes to T_2 and hence the appearance of the tissues.

There may be other effects that can lead to manipulation of the dipolar coupling relaxation mechanisms. These include the possibilities raised by so-called RF magic angle spinning (29). This will not be discussed further here since the technique is still a long way from application in clinical practice, and it is likely to be restricted by RF energy deposition. A few initial studies have looked at other methods associated with solid-state MR, such as the use of the magic sandwich echo (30). Both of these methods are designed to break the dipolar coupling through the use of RF pulse sequences.

Susceptibility Effects

Changing the timing of data acquisitions of tissue can have a very material effect on conspicuity when the dominant contrast mechanism is susceptibility. Susceptibility effects can be manipulated by altering the image matrix and slice width (31). As a consequence, T_2* requires the specification of voxel dimensions and the exact voxel location for which T_2* is being quoted. Reducing the time to the acquisition of the first data point allows susceptibility effects to be minimized. Intravoxel dephasing (which can result in loss of signal) is controlled by the relationship (ignoring the effects of T_2, whether multicomponent or not):

$$S_{dephase} = K\int \rho_r e^{iy\bar{o}BrTE}dr, \quad (9)$$

where ρ_r is the PD in the selected voxel, δB_r is the offset between the weighted mean field in the voxel and that at location r, and $S_{dephase}$ is the resultant signal. This relationship means that cubic voxels are less prone to artifacts from this source than highly asymmetrical ones of the same volume, such as those frequently required in order to get enough signal (through a thick slice) without losing in-plane imaging resolution through a limited acquisition matrix. Loss of signal is to be distinguished from the possible offset of resonance frequency of the voxel as a whole, leading to phase offsets that are sometimes mapped. This is given by:

$$\Phi_o = \gamma\delta B_0 TE \quad (10)$$

where Φ_o is the phase deviation of the voxel when the mean field in the voxel is offset from the reference field by δB_0. Susceptibility dephasing occurs with GRE sequences, and is considerably reduced with SE data acquisitions. While dephasing due to susceptibility effects can be reversed using a refocusing pulse, as in a standard SE sequence, dephasing due to susceptibility will occur throughout the data acquisition and limit the spatial resolution.

Susceptibility effects result in a transverse relaxation time T_2*, which at most is as long as T_2 and may be very much shorter. The two forms are related through $T_2^* = 1/(1/T_2 + R)$, where R is the effective relaxation rate due to susceptibility. This implies that T_2* relaxation is exponential. While in general this is not true, it does provide an interpretive formalism. When susceptibility effects are significant compared to T_2 relaxation, and the data are acquired using a GRE sequence, then T_2* is the correct notation.

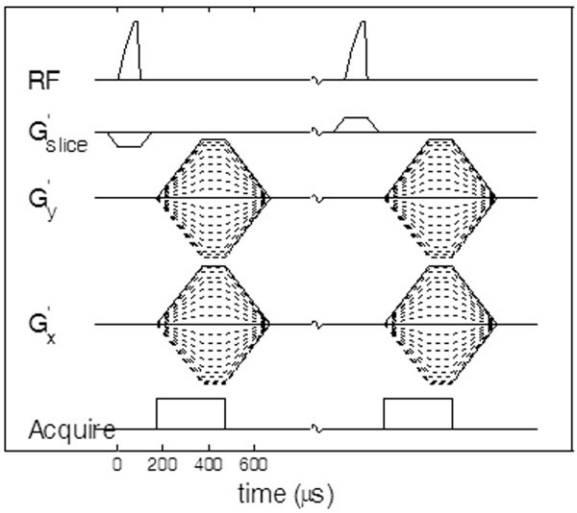

Figure 4. Pulse sequence diagram for a basic UTE sequence. The half-RF pulses are applied with the slice-selection gradient G'_z negative in the first half and positive in the second half. The RF pulse is truncated and followed rapidly by the acquisition, during which G'_x and G'_y are applied to obtain the radial gradient. These gradients ramp up to a plateau during data acquisition.

One example of the differing behavior of components with similar short T_2s arising from separate mechanisms is the application of excitation pulses. This is because with susceptibility effects, the individual ρ_r described above may have long T_2s and hence will be excited in the same manner as the components exploited in conventional MRI by the excitation pulses (i.e., $\alpha = \beta$ in Eq. [1]). The net consequence of this is that the material behaves as the ensemble of many small samples, each with a narrow line shape but at different frequencies. For this reason the excitation of short T_2* species does not necessarily follow the general excitation behavior of short T_2 species.

UTE PULSE SEQUENCES

Many of the techniques used for the rapid acquisition of data are not useful for short T2 tissues. The major multiecho methods (rapid acquisition with relaxation enhancement (RARE) (32) and echo-planar imaging (EPI) (33)) are not useful because they depend on tissues having a relatively long T_2 to maintain the utility of their multiple data acquisitions. SE methods generally present problems because it is difficult to produce an effective 180° refocusing pulse for short T_2 relaxation components. The fast acquisition method of most value is likely to be turbo fast low-angle shot (Turbo-FLASH) (34) and its variants.

A useful approach is one based on radial traverses of k-space starting in the center (35,36). Acquisition on the gradient ramp using nonlinear sampling (37) minimizes the TE. The radially sampled data points can subsequently be interpolated onto a rectangular matrix, and conventional two-dimensional Fourier transform (2DFT) processing can be used to form the image.

To achieve even shorter times for the excitation process, it is necessary to avoid the use of a slice rephasing gradient. This can be achieved by using a nonselective pulse to acquire 3D data, and using the sensitivity profile of the RF coils to restrict the region over which signals are acquired.

An alternative in a 2D imaging experiment is to excite the slice in two stages, and acquire half of the k-space content of the slice profile each time using gradients with opposite senses (38). If the excitation process is arranged to terminate rapidly, data acquisition can be started at the center of k-space almost immediately. The two data acquisitions are then added together to give the complete data content. An image requires a minimum of 2mTR to acquire, where m is the number of radial lines to be acquired. The pulse sequence is illustrated in Fig. 4.

One of the disadvantages of radial data acquisition is that it samples a square field of view (FOV) rather inefficiently. In practice, full coverage using center-out of an $n \times n$ pixel image requires $n\pi$ acquisitions (rather than the n data acquisitions used in conventional rectangular sampling) or $n\pi/2$ if the data are sampled from the center and conjugate reflection is used. An unintended bonus of this requirement is that the center of k-space is consequently oversampled, and low spatial frequencies of the image have a better signal-to-noise ratio (SNR) than high frequencies.

Other short-TE pulse sequences, such as single-point ramped imaging with T1 enhancement (SPRITE) (39), 3D constant time (40) multipoint acquisitions (41), continuous wave methods (42), and swept frequency imaging (43), have been used in solid-state or semi-solid-state applications in in vitro studies. These techniques show considerable promise, although they have yet to be employed in patient studies.

CLINICIAL APPLICATIONS

The signal from tissues is typically multiexponential, with protons in proteins and in water tightly bound to proteins having T_2s of about 10 μs. The T_2 of protons in water, which is less tightly bound, increases into the clinical range.

Using standard SE sequences, tissues with a T_2 significantly shorter than 10 msec are not detectable with basic clinical MR systems, though with more modern instruments using gradient echoes the limit is probably closer to 1–2 msec.

From a clinical point of view, it is useful to divide tissues into two general groups: those with a majority of short T_2 components (Table 2) and those with a minor-

Table 2
Tissues With a Majority of Short T_2 Components

Meninges (dura)	Falx	Tentorium
Membranes	Capsules	Bands
Retinaculi	Septae	Fascae
Sheaths	Nails	Hair
Aponeuroses	Tendons	Ligaments
Menisci	Labrii	Periosteum
Bone	Dentine	Enamel

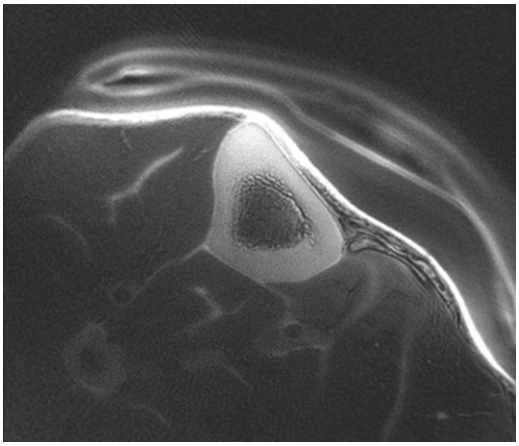

Figure 5. Normal cortical bone. Difference UTE image (IR = 500/0.08 minus 4.5/250 msec at 1.5T, resolution = 512 × 512, FOV = 14 cm). The cortical bone is highlighted.

ity. The tissues with a majority often produce no signal or a very low signal using conventional clinical pulse sequences. The most common mechanism of relaxation is dipolar dephasing. The remainder of tissues have a variable content of short T_2 components. For example, short T_2 components may be more prominent in white matter in association with myelin than in gray matter.

In disease, the concentration of short T_2 components may increase or decrease. The relaxation times T_1 and T_2 may also increase or decrease. In general, an increase in the T_2 is conventionally observed in a long T_2-weighted sequence is accompanied by a decrease in signal from short T_2 components. Diseases that increase the concentration of short T_2 components include fibrosis (chronic), iron deposition, some stages of hemorrhage, some stages of calcification, and various deposition diseases (e.g., amyloidosis). Cellular infiltration may also increase the concentration of short T_2 components. More common is a reduction in the concentration of short T_2 components due to edema, infiltration, tumors, and other conditions. This produces a loss of signal from short T_2 components on the images that are derived from subtracting images obtained at different TEs from each other ("difference images").

In general terms, imaging of tendons, ligaments, menisci, periosteum, cortical bone, and other short T_2 tissues has essentially involved low- or very-low-signal structures. Such structures are now detectable with the use of UTE techniques. This approach provides new options to characterize tissue and to employ different pulse sequences to change tissue conspicuity.

A variety of sequences were used to acquire the data presented below. The timings for the sequences are given in milliseconds in the figure legends (i.e., a TE of 0.08 means 80 μs). For the UTE sequences, we followed the convention of using the TE to describe the time from the end of the RF excitation to the beginning of data acquisition, although this is an oversimplification (44).

Cortical bone is of particular interest (Fig. 5). Study of this tissue puts a premium on quantification, as is the case with existing techniques for bone densitometry. T_1 increases significantly with age. Signal is available from both protons, which may reflect the organic matrix, and phosphorus, which may be more closely linked to calcium hydroxyapatite and reflect more closely what is seen with conventional x-rays or x-ray-based densitometry. Trabecular bone can also be seen (Fig. 6).

Contrast agents offer new options when combined with UTE techniques through decreasing T_1. Signal is now available from tendons, ligaments, and similar tissues, and this may be used to demonstrate enhancement (6–8). The very short T_2 tissues previously provided no signal before or after enhancement. The increase in signal due to the use of the UTE acquisition at the shortest value of TE is a function of the T_2 of the tissue and the delay to the TE. A particular advantage of gadolinium (Gd) chelates is that they enable one to simultaneously detect increased signal in a short T_2 component tissue, and suppress the signal from long T_2 tissues and fluids. With magnetic iron-oxide particles, the same general principles apply.

The difference image may also be of value because it combines the anatomy from the first UTE echo with the susceptibility contrast in the subsequent echo at a longer TE. The meniscus is of particular interest. Despite intensive efforts, investigators have not been able to distinguish the red from the white zone of the meniscus, or to detect contrast enhancement in either zone. However, one can now achieve such a distinction with UTE pulse sequences by using subtraction to selectively reduce the signal from the adjacent perimeniscal tissues (6–8).

The normal periosteum is a tissue of 1–2 mm thickness that surrounds the cortical bone and is important for bone nutrition and healing in fractures (Fig. 7). It was previously undetectable in adults by MRI, but it now can be seen with UTE sequences and shows enhancement after fractures. The deep layer of articular cartilage can be seen (Fig. 8). Calcification may have a

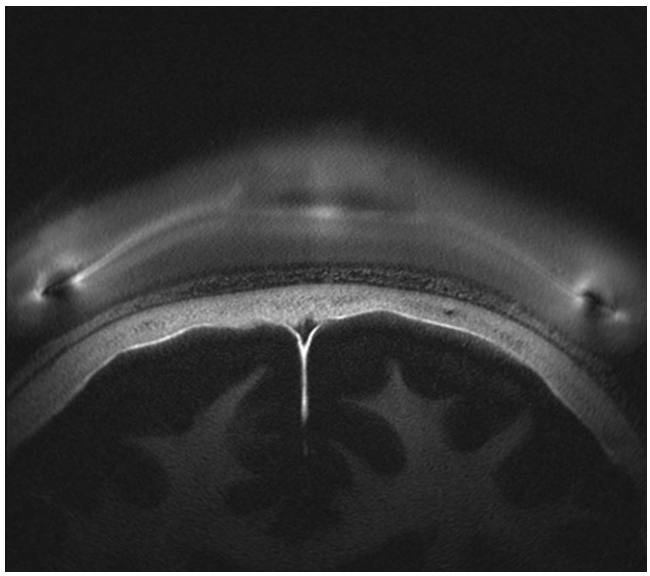

Figure 6. Trabecular bone (IR = 500/0.08 minus 4.5/200 msec at 1.5T, resolution = 512 × 512, FOV = 14 cm). Difference UTE image of the skull. Trabecular bone can be seen between the inner and outer tables.

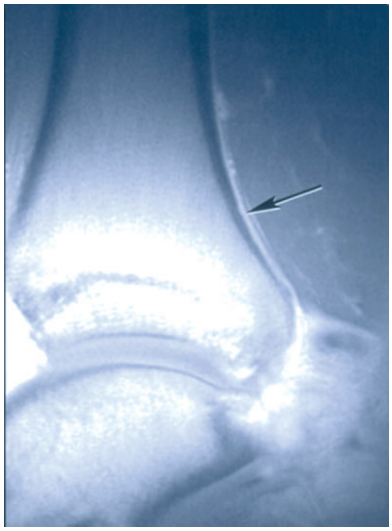

Figure 7. Periosteum, seen in the lower end of the tibia (arrow) (UTE = 500/0.08 msec at 1.5T, resolution = 512 × 512, FOV = 14 cm).

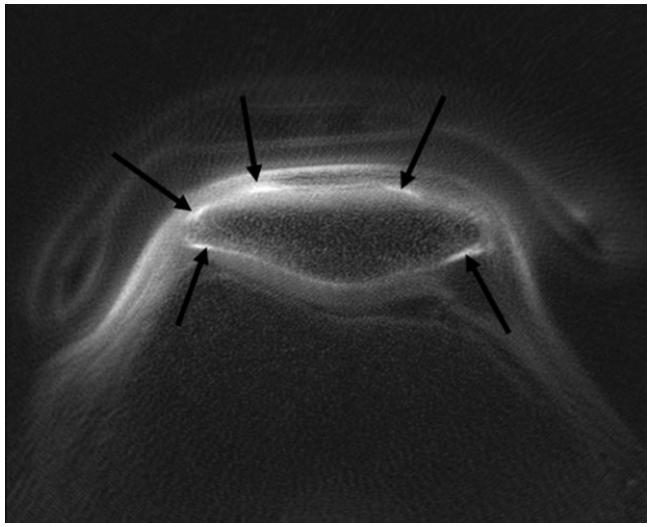

Figure 9. Transverse image of the patellar showing calcification. Fat-suppressed UTE image (TR/TE = 500/0.08 msec at 1.5T, resolution = 512 × 512, FOV = 12 cm). The calcified tissue has a high signal (arrows).

high signal (Fig. 9). In the brain, short T_2 components in the white matter can be selectively imaged. The short T_2 components in the meninges and in certain diseases, such as malignant melanoma, can also be detected (Fig. 10).

MR SYSTEM ISSUES

It is reasonable to ask what sort of modifications are needed to make clinical MRI systems useful for evaluating short T_2 components of tissue, and whether specialized machines may be useful for studying tissues such as tendons, ligaments, and cortical bone.

Level of B_0

Given the limited possibilities for the use of fast imaging methods and the fact that even multislice acquisitions may be difficult, one might assume that higher B_0 fields with consequent SNR improvements would be desirable. However, the disadvantages of higher field strength include an increase in T_1 and decreased options for the application of RF pulses owing to the additional SAR constraints. As such, low-field systems (with consequently shorter T_1s) may offer advantages. Further, the primary contrast mechanism that is available for manipulation in UTE is T_1, and the range of values of T_1 is reduced at very high fields.

It is much easier to image less abundant nuclei, such as phosphorus and sodium, at higher fields. If there is value in the use of very short TE imaging for proton studies, it is that there will likely be gains from studies using other nuclei. Generally, the hardware issues are very similar, apart from the complication of needing dual-channel RF systems. It is likely that in UTE imaging, the "optimum" field strength will depend on the exact area of application.

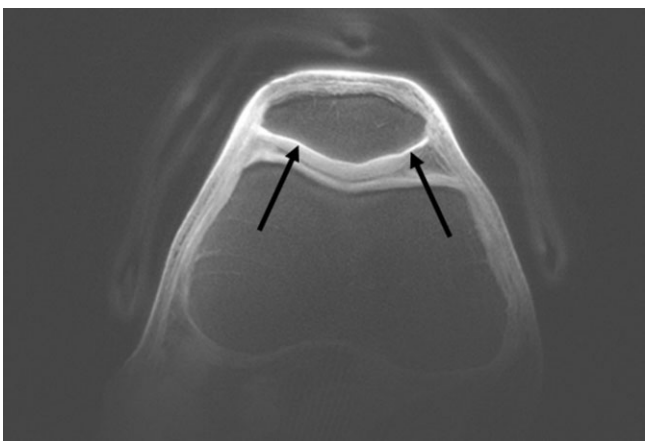

Figure 8. Normal patellar cartilage UTE (TR/TE = 500/0.08 msec at 1.5T, resolution = 512 × 512, FOV = 12 cm) image. The deep layer of the cartilage is highlighted (arrow).

Gradient System

The gradient performance (i.e., slew rates and amplitudes) should be as high as possible. It is desirable to ramp down the slice-selection gradients very quickly, since any lag between the end of the RF excitation and the end of the slice-select gradient results in signal dephasing. The alternative of this is to begin ramping down the slice-selection gradient during RF excitation. However, this approach can cause excitation of spins outside the desired slice, and it may not be possible to correct this precisely (although the variable rate selective excitation (VERSE) method (45) can reduce these out-of-slice errors to a minimum). This slice selection requires careful attention when imaging faint signals in the presence of strong out-of-slice signals (e.g., beneath a surface coil). The additional acquisitions used in the half-pulse method make it sensitive to errors caused by eddy currents, because they are established by opposite-polarity slice-selection gradients.

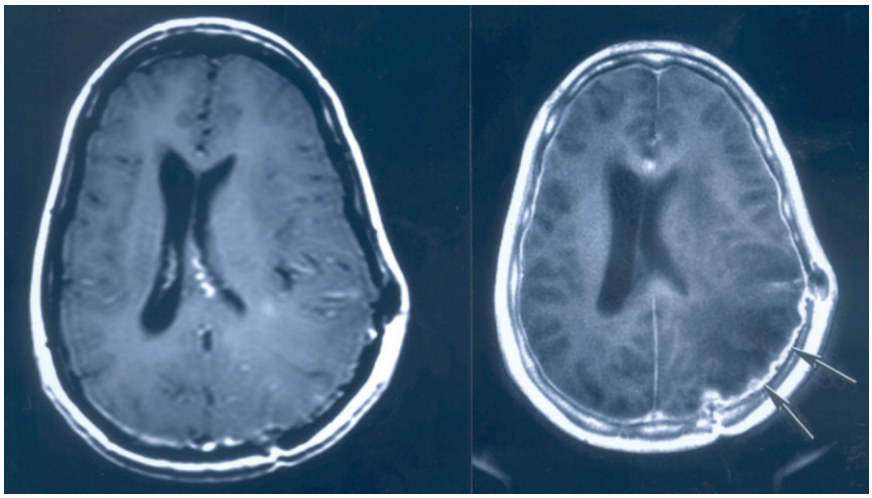

Figure 10. Malignant melanoma metastases to the brain. Transverse conventional 2DFT (left; TR/TE = 500/20.0 msec, matrix = 256 × 512) and difference UTE (right; TR/TE = 500/0.08, matrix = 512 × 512) images, both obtained at 1.5T. The meninges is thickened and much more obvious on the UTE image (arrows).

The other fast gradient operation is performed during data collection. In practice, data must be collected as the acquisition gradients are ramped up, with the use of nonlinear sampling. A sinusoidal or other gradient shape can be used, and constant gradient level is not necessary. With nonlinear sampling, the first data point can be acquired before the encoding gradient is actually present, as was the custom for at least one of the early MRI systems (46). A delicate synchronization of acquired data with regridding is therefore required, which is sensitive to timing errors of 1 μs and can be problematic for oblique imaging if gradient axes have even slightly different temporal responses. Therefore, gradient systems for UTE should be self-shielded and have reproducible, well-characterized behavior, and should be identical for each gradient axis.

A second criteria for the acquisition gradients relates to the period for which data are recovered. In practice, data should be recovered for as long as possible (within machine constraints), or for as long as the T_2 (or T_2*) permits. In the latter situation, an optimal SNR is obtained from acquisitions in which data are recovered for a duration on the order of T_2. Based on tissue T_2 values measured during our studies, we believe a useful target for the data acquisition would be a duration (t_{acq}) of 250 μs. Assuming a 300-mm FOV (V), and a matrix size (M) of 256, the minimum gradient amplitude (G_{min}) needed is given by:

$$G_{min} = \pi M/\gamma t_{acq} V \qquad (11)$$

G_{min} = 40 mT/m for the above parameters. However, G_{min} assumes a square gradient pulse, which is impossible to achieve in reality. With a rise time of 75 μs, the actual gradient strength would have to be ~57 mT/m. dB/dt would then be 228 T/second at 300 mm from the machine axis. It may be that a minimum duration of 350 μs will have to be accepted for regulatory reasons as far as whole-body coils are concerned.

Substantially higher rates of change of field can be obtained from localized coils, in which the gradients are of limited physical extent. Head-only coils, with which dB/dt figures of 600–1000 T/m/s are achievable, are a case in point. However, as far as UTE imaging is concerned, confining its use to the brain and the extremities may prove unduly restrictive.

RF System

A major requirement for the RF receiver system is that it should recover very quickly. High-resolution spectrometers have recovery times of <1μs, since it is important that they do not lose data from solid samples. Fast switching between transmit and receive modes has not been a major requirement in clinical MRI, but it is likely to become more important as TE is reduced toward zero. This will have an impact on detector coils. Such coils are likely to be saturated by the excitation RF pulses, and (particularly if they are of high Q) require time to recover. As mentioned above, the slice-selection method used and the limited possibilities for the use of fast acquisition methods mean that two excitations will be needed. One possible approach for reducing the total acquisition time in this case is to use partial parallel imaging strategies, such as sensitivity encoding (SENSE) (47) and simultaneous acquisition of spatial harmonics (SMASH) (48). The use of large arrays of small, fairly low Q coils could then become an attractive option.

Higher peak RF transmitter fields than are currently in use will be desirable. Hard pulses have to be genuinely hard, so a useful target might be to achieve a 180° pulse in 10 μs for proton imaging. This means that peak B_1 should be on the order of 1.2 mT. This level of RF, while of great interest for $T_{1\rho}$ studies, is likely to cause safety regulators concern, and will require even more precise monitoring of the RF load delivered to the patient than is done already. The RF power amplifier levels required by this target for whole-body operation are extreme, and will require a major engineering effort. Therefore, it is likely that these B_1 levels will normally be generated only over small regions of the body.

Data Processing

UTE imaging requires very high sampling rates. Substantial oversampling is desirable to facilitate the use of nonlinear sampling or a much faster sampling rate. In

Refs. 29 and 30, the actual rate at which samples were acquired varied by more than a factor of 10, and with a mean sampling time in the range of 5–10 μs and a temporal resolution of 100 ns, the total acquisition time was 10–100 msec. To acquire UTE data, one could use oversampling instead of varying the rate of sampling, and the samples could be retrospectively selected, interpolated, and aggregated. Thus, with a target mean sample interval of 1 μs, the true sampling rate would be at least 4 MHz, and preferably 5 MHz or more.

Safety

While B_0 levels are unlikely to raise any new concerns, both the gradient field switching levels and particularly the RF fields suggested here are likely to present safety challenges.

The proposed RF excitation field level is not technically impossible to achieve, particularly if dedicated transmitter coils are used. It must be remembered that the RF field power level increases as the square of its amplitude. However, for a given flip angle, the actual total power increases linearly with the field amplitude because the duration of the exciting pulse falls as its amplitude is increased. On the other hand, spin-locking methods use long pulses, and the maximum available amplitude is likely to be needed for relatively long times. The mean power deposited can be reduced by very large increases in TR or by the use of substantially lower levels of B_0. Safety limits are actually a moving target, with levels often set by regulators in the absence of experimental data. In the past, engineers have pushed at these limits; clinicians have found a use for the facilities on offer, and, for want of contraindications, in time the regulators have tended to relax limits. Thus the upper field limit (B_0) has risen from 2T to 4T, with investigational device exemptions as high as 9.4T. Gradient strength limits have risen from 10 mT/m to 60 mT/m or more. Only RF limits, for which there are more experimental data, have remained relatively stable, although safety issues are subject to ongoing debate (49).

CONCLUSIONS

UTE imaging has considerable potential and will benefit from new tailored equipment to maximize its performance. The clinical utility of this approach has yet to be established, but the initial results are promising enough to justify further development.

REFERENCES

1. Bergin CJ, Pauly JM, Macovski A. Lung parenchyma: projection reconstruction imaging. Radiology 1991;179:777–781.
2. Bergin CJ, Noll DC, Pauly JM, Glover GH, Macovski A. MR imaging of lung parenchyma: a solution to susceptibility. Radiology 1992; 183:673–676.
3. Gold GE, Pauly JM, Macovski A, Herfkens RJ. MR spectroscopic imaging of collagen: tendons and knee menisci. Magn Reson Med 1995;34:654–674.
4. Schmidt MA, Yang GZ, Gatehouse PD, Firmin DN. FID-based lung MRI at 0.5T: theoretical considerations and practical implementation. Magn Reson Med 1998;39:666–672.
5. Gatehouse PD, Bydder GM. Magnetic resonance imaging of short T_2 components in tissue. Clin Radiol 2003;58:1–19.
6. Robson MD, Gatehouse MD, Bydder M, Bydder GM. Magnetic resonance: an introduction to ultrashort TE (UTE) imaging. J Comp Assist Tomogr 2003;27:824–846.
7. Gatehouse PD, Thomas RW, Robson MD, Hamilton G, Herlihy AH, Bydder GM. Magnetic resonance imaging of the knee with ultrashort TE pulse sequences. Magn Reson Imaging 2004;22:1061–1067.
8. Robson MD, Benjamin M, Gishen P, Bydder GM. Magnetic resonance imaging of the achilles tendon using ultrashort TE (UTE) pulse sequences. Clin Radiol 2004;59:727–735.
9. Reichert IL, Robson MD, Gatehouse PD, et al. Magnetic resonance imaging of cortical bone with ultrashort TE pulse sequences. Magn Reson Imaging 2005;23:611–618.
10. Chappell KE, Patel N, Gatehouse PD, et al. Magnetic resonance imaging of the liver with ultrashort TE (UTE) pulse sequences. J Magn Reson Imaging 2003;18:709–13.
11. Waldman A, Rees JH, Brock CS, Robson MD, Gatehouse PD, Bydder GM. MRI of the brain with ultra-short echo-time pulse sequences. Neuroradiology 2003;45:887–892.
12. Hall-Craggs MA, Porter J, Gatehouse PD, Bydder GM. Ultrashort echo time (UTE) MRI of the spine in thalassaemia. Br J Radiol 2004;77:104–110.
13. Reichert IL, Benjamin M, Gatehouse PD, et al. Magnetic resonance imaging of periosteum with ultrashort TE pulse sequences. J Magn Reson Imaging 2004;19:99–107.
14. Robson MD, Gatehouse PD, Bydder GM, Neubauer S. Human imaging of phosphorus in cortical and trabecular bone in vivo. Magn Reson Med 2004;51:888–892.
15. Ernst RR, Anderson WA. Application of Fourier transform spectroscopy to magnetic resonance. Rev Sci Instrum 1996;37:93–102.
16. Sussman MS, Pauly JM, Wright GA. Design of practical T_2-selective RF excitation (TELEX) pulses. Magn Reson Med 1998; 40:890–899.
17. Crooks L, Arakawa M, Hoenninger J, et al. Nuclear magnetic resonance whole-body imager operating at 3.5 K Gauss. Radiology 1982;143:169–174.
18. Kucharczyk W, Crawley AP, Kelly WM, Henkelman RM. Effect of multislice interference on image contrast in T_2- and T_1- weighted MR images. ANJR Am J Neuroradiol 1987;9:443–451.
19. Santyr GE. Magnetization transfer effects in multislice MR imaging. Magn Reson Med 1993;11:521–532.
20. Wolff SD, Balaban RS. Magnetization transfer contrast (MTC) and tissue water proton relaxation *in vivo*. Magn Reson Med 1989;10: 135–144.
21. Haase A, Frahm J, Hanicke W, Matthaei D. ^{1}H NMR chemical shift selective (CHESS) imaging. Phys Med Biol 1985;30:341–344.
22. Abragam A. Principles of nuclear magnetism. Oxford, UK: Clarendon Press; 1961. p 511–539.
23. Forsen S, Hoffman RA. Study of moderately rapid chemical exchange reactions by means of nuclear magnetic double resonance. J Appl Phys 1963;30:2892–2901.
24. Sepponen RE, Pohjonen JA, Sipponen JT, Tanttu JI. A method for $T_{1\rho}$ imaging. J Comput Assist Tomogr 1985;9:1007–1011.
25. Abragam A. Principles of nuclear magnetism. Oxford, UK: Clarendon Press; 1961. p 289–305.
26. Fullerton GD, Cameron IL, Ord VA. Orientation of tendons in the magnetic field and its effects on T_2 relaxation times. Radiology 1985;155:433–435.
27. Henkelman RM, Stanisz GJ, Kim JK, Bronskill MJ. Anisotropy of NMR properties of tissues. Magn Reson Med 1994;32:592–601.
28. Marshall H, Howarth C, Larkman DJ, Herlihy AH, Oatridge A, Bydder GM. Contrast enhanced magic angle MR imaging of the achilles tendon. AJR Am J Roentgenol 2002;179:192–197.
29. De Luca F, Nuccetelli C, De Simons BC, Maraviglia B. NMR imaging of a solid by the magic-angle rotating-frame method. J Magn Reson 1986;69:496–500.
30. Grenier D, Pascui O, Briguet A. Dipolar contrast for dense tissues imaging. J Magn Reson 2000;147:353–356.
31. Young IR, Cox IJ, Coutts GA, Bydder GM. The benefits of increasing spatial resolution as a means of reducing artifacts due to field in homogeneities. Magn Reson Imaging 1988;6:585–590.
32. Hennig J, Nauerth A, Friedburg H. RARE imaging: a fast imaging method for clinical MR. Magn Reson Med 1986;3:823–833.
33. Mansfield P. Multi-planar image formation using NMR spin echoes. J Phys C Solid State Phys 1977;10:L55–L58.
34. Haase A. Snapshot FLASH MRI, applications to T_1, T_2 and chemical-shift imaging. Magn Reson Med 1990;13:77–89.

35. Young IR, Bailes DR, Burl M, et al. Initial clinical evaluation of a whole body nuclear magnetic resonance (NMR) tomograph. J Comput Assist Tomogr 1982;6:1–18.
36. Young IR, Bailes DR, Collins AG, Gilderdale DJ. Image options in NMR. In: Witcofski RL, Karstde N, Partain CL, editors. NMR imaging. Winston-Salem: Bowman Gray School of Medicine, Wake Forest University; 1982. p 93–100.
37. Clow H, Percival WS. Non-linear sampling in NMR. U.S. patent 4315216; 1978.
38. Pauly JM, Conolly SI, Nishimura D, Macovski A. In: Proceedings of the 8th Annual Meeting of ISMRM, Amsterdam, The Netherlands, 1989 (Abstract 28).
39. Balcom BJ, Macgregor RP, Beyea SD, Green DP, Armstrong RL, Bremner JW. Single-point ramped imaging with T1 enhancement (SPRITE). J Magn Reson A 1996;123:131–134.
40. Wu Y, Chester DA, Glimcher MJ, et al. Multinuclear solid-state three dimensional MRI of bone and synthetic calcium phosphates. Proc Natl Acad Sci USA 1999;96:1574–1578.
41. Fernandez-Seara MA, Wehrli SL, Wehrli FW. Multipoint mapping for imaging of semi-solid materials. J Magn Reson 2003;160:144–150.
42. Fagan AJ, Davies GR, Hutchison JM, Glasser FP, Lurie DJ. Development of a 3-D, multi-nuclear continuous wave NMR imaging system. J Magn Reson 2005;176:140–150.
43. Idiyatullin D, Corum C, Park JY, Garwood M. Fast and quiet MRI using a swept radiofrequency. J Magn Reson 2006;181:342–349.
44. Robson MD, Gatehouse PD, Young IR, Bydder GM. Ultrashort TE (UTE) imaging of short T2 components: how should the T2 weighting be described? In: Proceedings of the 12th Annual Meeting of ISMRM, Kyoto, Japan, 2004 (Abstract 636).
45. Conolly S, Nishimura D, Macovski A. Variable-rate selective excitation. J Magn Reson 1988;78:440–457.
46. Glover GH, Pauly JM. Projection-reconstruction in MR. In: Young IR, editor. Methods in biomedical magnetic resonance imaging and spectroscopy. Chichester, UK: Wiley; 2000. p 225–231.
47. Preussman KP, Weiger M, Scheidegger MB, Boesiger P. Coil sensitivity encoding for fast MRI. In: Proceedings of the 6th Annual Meeting of ISMRM, Sydney, Australia, 1998 (Abstract 579).
48. Sodickson DK, Manning WJ. Simultaneous acquisition of spatial harmonics (SMASH): fast imaging with radiofrequency coil arrays. Magn Reson Med 1997;38:591–603.
49. Keevil SF, Gedroyc W, Gowland P, et al. Electromagnetic field exposure limitation and the future of MRI. Br J Radiol 2005;78:973–975.